Materials Research Innovations

ISSN: 1432-8917 (Print) 1433-075X (Online) Journal homepage: http://www.tandfonline.com/loi/ymri20

Facile synthesis of porous cobalt oxide microplates and their lithium ion storage properties

H. Che, A. Liu, C. Liu, R. Jiang, Q. Fu, C. Wang & L. Wang

To cite this article: H. Che, A. Liu, C. Liu, R. Jiang, Q. Fu, C. Wang & L. Wang (2014) Facile synthesis of porous cobalt oxide microplates and their lithium ion storage properties, Materials Research Innovations, 18:5, 380-385

To link to this article: http://dx.doi.org/10.1179/1433075X13Y.0000000168

Published online: 06 Dec 2013.

Facile synthesis of porous cobalt oxide microplates and their lithium ion storage properties

H. Che*, A. Liu, C. Liu, R. Jiang, Q. Fu, C. Wang and L. Wang

Porous cobalt oxide (Co_3O_4) microplates have been successfully synthesised via a facile thermal decomposition from plate-like cobalt oxalate complex precursors. The microstructures and morphologies of the obtained Co_3O_4 materials are characterised by X-ray diffraction, scanning electron microscopy, transmission electron microscopy and N_2 adsorption–desorption techniques. The characterisation results show that the obtained Co_3O_4 microplates are composed of plate-like polycrystalline nanoparticles with lengths of ~20 nm and widths of ~10 nm. In addition, these nanoplates aggregate each other to form the porous network with an average pore size of ~18·9 nm. The obtained porous Co_3O_4 microplates exhibit high discharge–charge capacities and good rate performances, suggesting a promising application as anode materials for Li ion batteries.

Keywords: Porous, Cobalt oxide, Plates, Anode materials, Li ion battery

Introduction

Porous transition metal oxides have attracted considerable attention due to their low bulk density, large surface area and surface permeability. Such materials have potential applications in many fields such as catalysis,[1,2] sensors,[3,4] batteries materials,[5] etc. Among them, porous cobalt oxide (Co_3O_4) materials have drawn much interest over the past decade due to their application as magnetic materials,[6] heterogeneous catalysts,[7] gas sensors,[8] supercapacitors[9] and rechargeable lithium ion batteries (LIBs).[10,11] Up to now, various methods have been reported to prepare porous Co_3O_4 with different morphologies like belts,[12] rods,[13] flowers,[14] cubes,[15] tubes,[16] wires,[17] microspheres[18] and so on. Among them, the templating method is generally used to synthesise porous Co_3O_4, including the soft templates such as biological templates,[19] surfactants,[20] block copolymers[21] and hard templates, for example anodised alumina membranes,[22] carbon microspheres[23] or mesoporous silica.[24] However, the use of templates usually suffers from some disadvantages such as tedious synthetic procedures, high cost and low field. As a result, this may prevent them from large scale production. Therefore, great efforts are being paid worldwide to potentially more effective and economical methods for the preparation of porous Co_3O_4.

More recently, the thermal decomposition from cobalt based precursors such as cobalt hydroxides, cobalt nitrate hydroxides, carbonates, oxalates, carbonate hydroxides precursors, etc. has been reported to synthesise porous Co_3O_4 materials.[25–29] Compared with the templating methods, this method does not require complicated synthetic conditions or tedious post-treatment procedures such as the removal of templates by selective etching. In addition, chief among its advantages is simplicity. Therefore, such a strategy would become one of the most important methods for fabricating the porous transition metal oxides.

Herein, we describe a facile template free synthesis of porous Co_3O_4 microplates via the thermal decomposition from the disc-like complex precursor containing cobalt, oxalate, water and alcohol, which is firstly prepared using the solvothermal method. The obtained porous Co_3O_4 microplates exhibit a higher reversible capacity and a good recycling performance, providing a potential application as anode materials for LIBs.

Experimental

All of the reagents were purchased from Sinopharm Chemical Reagent Co., Ltd. Moreover, they were of analytical grade and used without further purification. In a typical synthesis of porous Co_3O_4 microplates, 1·0 g of $Co(NO_3).6H_2O$ was dissolved in 40 mL of anhydrous alcohol under vigorous magnetic stirring. Then, 9·0 mL of 0·5 mol L^{-1} $(NH_4)_2C_2O_4$ aqueous solution was added into the alcohol solution. After stirring for 30 min, the obtained pink slurry was transferred and sealed tightly in a 100 mL Teflon lined steel autoclave, heated at 100°C for 24 h, and finally cooled to room temperature. The pink precipitates were collected by filtration, washed alternately with deionised water and alcohol three times and dried at 60°C for 6 h. Finally, the as prepared precipitates were subjected to

Department of Materials Science and Engineering, College of Equipment Manufacturing, Hebei University of Engineering, Handan 056038, China

*Corresponding author, email hongweiche@hebeu.edu.cn

Received 10 May 2013; accepted 26 July 2013
DOI 10.1179/1433075X13Y.0000000168

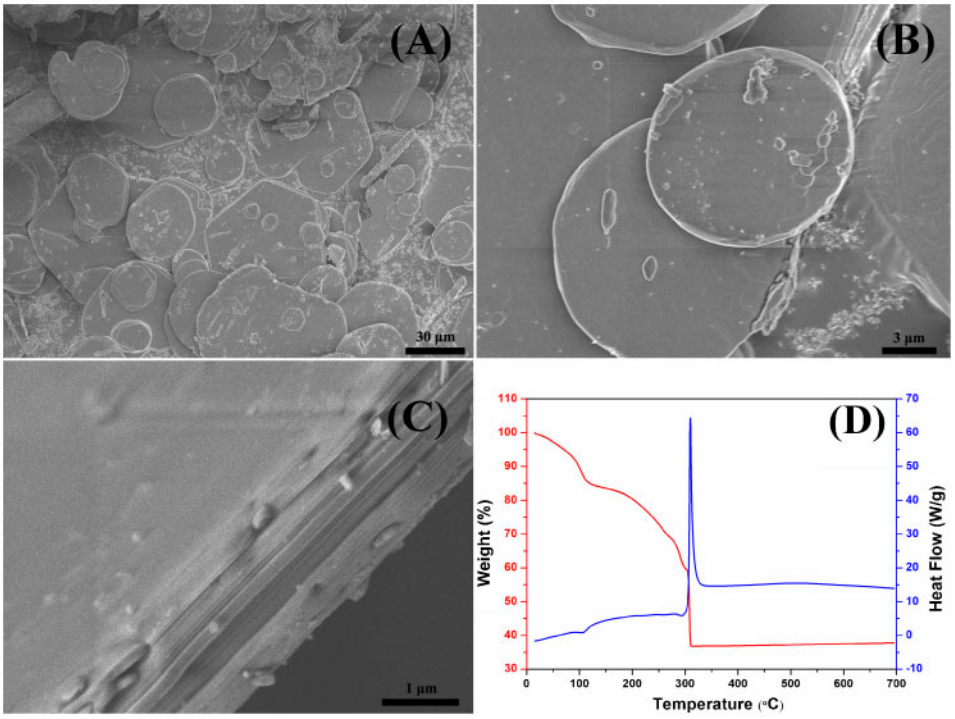

1 ***a–c*** **images (FE-SEM) and** ***d*** **differential scanning calorimetry thermogravimetric analysis (DSC-TGA) curve of pink precursors before calcination**

heat treatment in air at 350°C for 6 h with a heating rate of 2°C min^{-1}.

Characterisation

The wide angle X-ray diffraction patterns were recorded by a Bruker AXSD8 Advance X-ray diffractometer operated at 40 kV and 40 mA. Field emission scanning electron microscopy (FESEM) images were taken with a JSM-7600F field emission instrument. High resolution TEM (HRTEM) images and energy dispersive X-ray analysis were recorded using a JEM-2100 electron microscope operating at 200 kV. The sample was crushed in an agate mortar, dispersed in ethanol by ultrasonation and deposited on a microgrid. Nitrogen adsorption–desorption isotherms of the materials were determined at 77 K by a conventional volumetric technique with a Quantachrome Autosorb-1MP sorption analyser. Each sample was degassed at 573 K for 5 h under a pressure of 10^{-5} Pa or less. The surface area was calculated by the Brunauer–Emmett–Tell method, and the pore size distribution was evaluated by the Barrett–Joyner–Halenda (BJH) method. Weight changes of the products were measured out on a Thermal Analysis SDT Q600 analyser from 25 to 800°C under an air atmosphere at a heating rate of 10°C min^{-1}.

Electrochemical measurement

The working electrode was prepared by mixing the obtained porous Co_3O_4 microplates active materials, acetylene black and polyvinylidene fluoride in a weight ratio of 70 : 20 : 10 using *N*-methylpyrrolidone as the solvent. The resulting slurries were cast onto copper current collectors and then dried at 120°C under vacuum for 12 h. The foils were rolled into 30 μm thin sheets and then cut into discs, which were 14 mm in diameter. CR2016 coin type cells were assembled in an argon filled glove box with lithium foils as the counter electrodes and polypropylene microporous films (Celgard 2400) as separators. The liquid electrolyte was 1 mol L^{-1} of $LiPF_6$ in a mixture of ethylene carbonate and dimethyl carbonate (1 : 1, v/v). The galvanostatic charge and discharge tests were carried out by the CT2001A LAND testing instrument in a voltage range between 0·01 and 3·0 V at a current rate of 0·1, 0·5, 1 and 2 C (1 C=674 mA g^{-1}).

Results and discussion

The morphology of the as prepared pink precursors before calcination is firstly investigated by FESEM. The low magnification image in Fig. 1*a* displays that the precursors are mainly composed of plates with irregular circles or hexagonal shapes. The size of these plates is in the range of 10–100 μm. The magnified images (Fig. 1*b* and *c*) show that the surface of these microplates is very smooth, and their thickness is ~1·0 μm.

Figure 1*d* shows the DSC-TGA curve of the as prepared pink precursors. The total weight loss from room temperature to 320°C is 67·5%, which is significantly higher than 55·6% of the weight loss of cobalt oxalate ($CoC_2O_4.2H_2O$) in the same temperature range. In addition, the significant weight loss occurs <100°C for the pink precursors, but the weight loss is very slight for $CoC_2O_4.2H_2O$ in the same temperature range.[30] Considering that alcohol is used as the solvent in our synthetic procedure, the weight loss <100°C should be due to the evaporation from alcohol with a low boiling point. Therefore, it can be inferred that the as prepared pink precursors are probably described as the coordination complex ($CoC_2O_4.xH_2O.yC_2H_5OH$) composed of cobalt ion, oxalic ion, water and alcohol molecules. In addition, the formation reaction of $CoC_2O_4.xH_2O.yC_2H_5OH$ can be expressed as follows

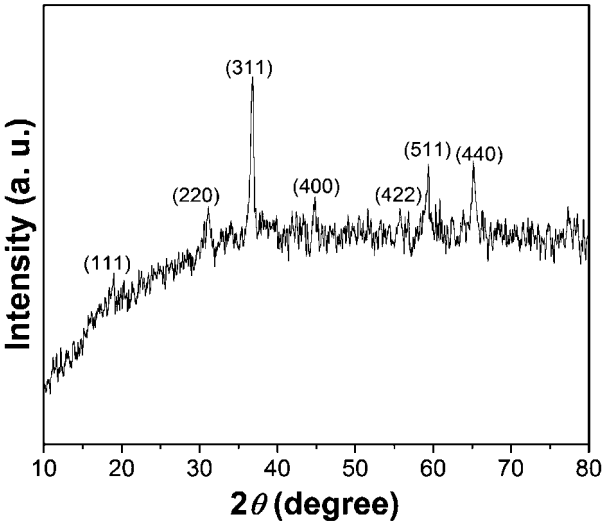

2 X-ray diffraction pattern of obtained products after calcination at 350°C for 6 h

$$Co^{2+} + C_2O_4^{2-} + xH_2O + yC_2H_5OH \rightarrow$$
$$CoC_2O_4.xH_2O.yC_2H_5OH(s)\downarrow$$

On the basis of the DSC-TGA data, the significant thermal decomposition takes place at ~310°C. Therefore, the as prepared precursors are calcined at 350°C to obtain pure Co_3O_4.

Figure 2 shows the X-ray diffraction pattern of the products after the pink crystal precursors are calcined at 350°C for 6 h. All the diffraction peaks can be indexed as a cubic spinel structure of Co_3O_4 (Joint Committee on Powder Diffraction Standards no. 42-1467). No other characteristic peaks for impurities are detected, confirming that the pink crystal precursors are completely transformed to Co_3O_4 after calcination at 350°C for 6 h. The corresponding average crystallite size is ~20 nm, calculated from the (311) peak of spinel structure by the Scherrer equation.

The morphology of the obtained Co_3O_4 products is characterised by FE-SEM, as is shown in Fig. 3. From the low magnification SEM image in Fig. 3*a*, it can be seen that the Co_3O_4 products exhibit the same plate-like morphology as the pink precursors before calcination. Moreover, their sizes and thicknesses have hardly been varied in comparison with the pink precursors. However, the magnified images in Fig. 3*b–d* indicate that the surface of these microplates becomes significantly rough, which is attributed to the thermal decomposition of the pink precursors into solid Co_3O_4, accompanying with the generation of CO_2 and H_2O gases. In addition, the small nanoparticles with irregular morphologies and sizes of ~20 nm aggregate each other, forming the porous structures. Such porous structures will be convenient and accessible for the diffusion of the electrolyte into the interior of Co_3O_4 microplates, which might improve their Li storage performances as anode materials for LIBs.

The microstructures and morphologies of the obtained Co_3O_4 products are further investigated by TEM and HRTEM. As is shown in Fig. 4*a*, nanopores are clearly revealed, surrounded by nanoparticles with size of ~20 nm, further confirming the above SEM characterisation. These nanoparticles exhibit a plate-like morphology with length of ~20 nm and width of ~10 nm, as is shown in Fig. 4*b*. The selected area electron diffraction taken from these plate-like nanoparticles in Fig. 4*c* clearly reveals the presence of (111), (220), (331), (400), (422), (511) and (440) diffraction rings and dots of spinel Co_3O_4 phase, proving the polycrystalline nature of Co_3O_4 nanoparticles, which is also in accordance with the X-ray diffraction data. The

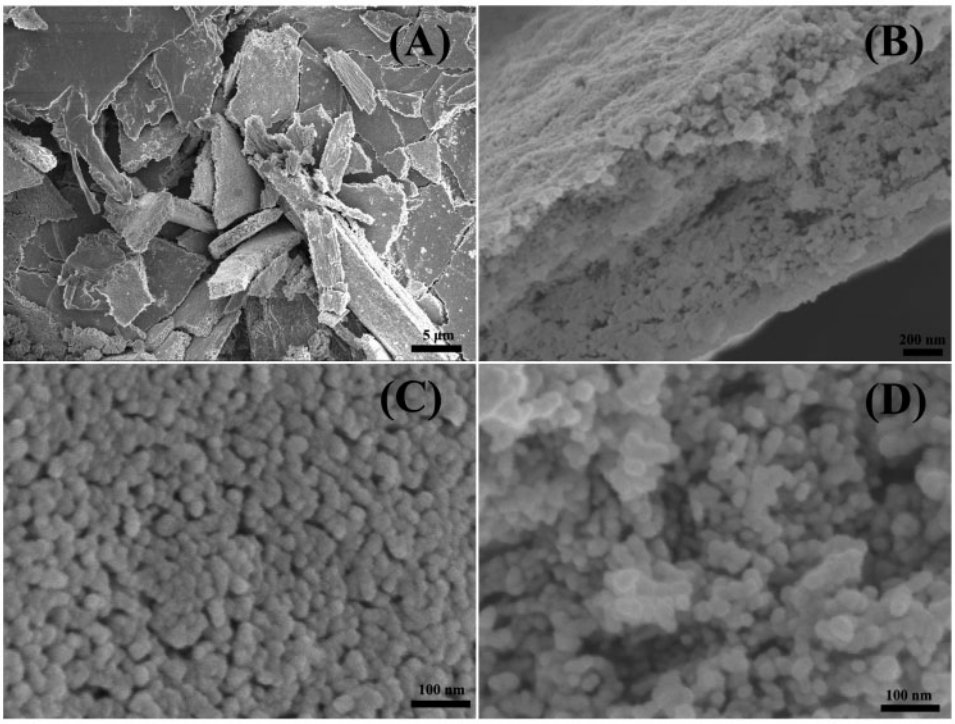

3 Images (FE-SEM) of obtained Co_3O_4 products after calcination at 350°C for 6 h

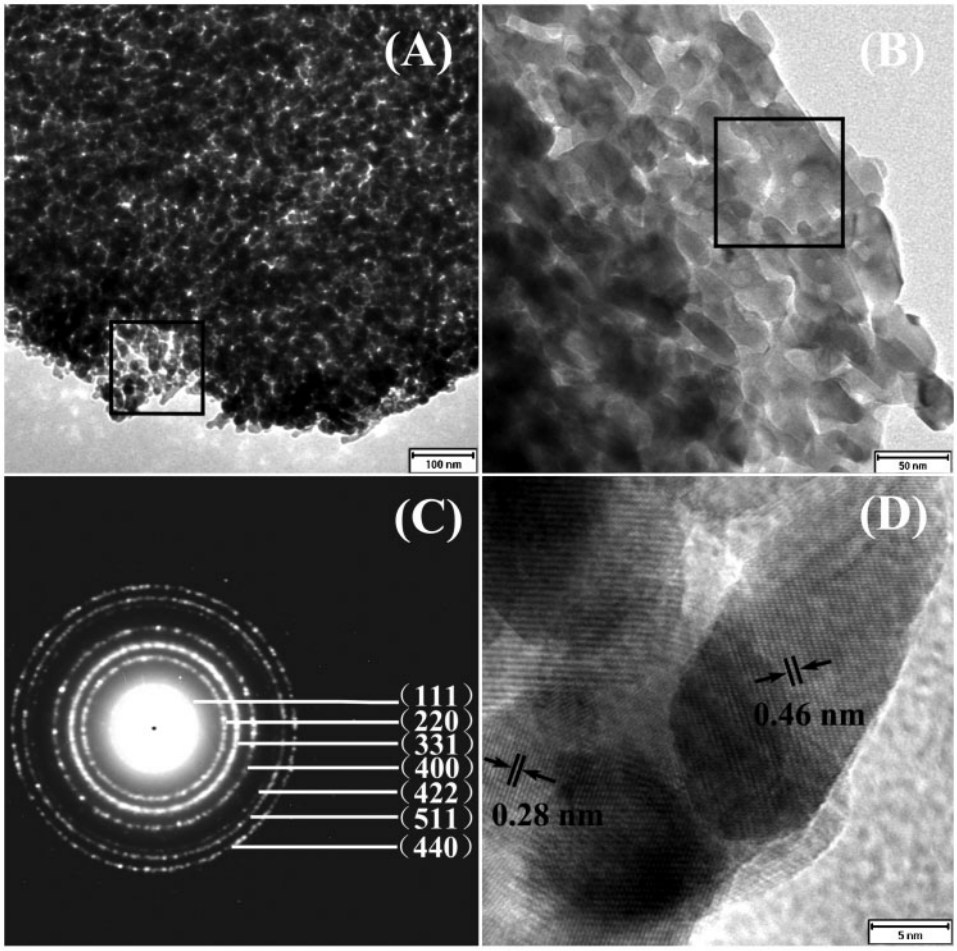

4 ***a, b*** **images (TEM),** ***c*** **selected area electron diffraction pattern and** ***d*** **HRTEM image of obtained Co_3O_4 products**

locally magnified HRTEM image corresponding to the square area in Fig. 4*d* clearly displays the lattice fringe, and the spacing of lattice fringes is ~0·28 and 0·46 nm, which can be indexed as the (220) and (111) planes of cubic spinel Co_3O_4 respectively.

Gas sorptometry measurement is conducted to confirm the inner architectures of the Co_3O_4 microplates. Figure 5 presents the N_2 adsorption/desorption isotherms and the corresponding BJH pore size distribution curve from the adsorption branch of the Co_3O_4 microplates. The isotherms can be classified as type IV, which is characterised by mesoporous materials. It agrees well with the results examined by the above SEM and TEM images. The Brunauer–Emmett–Tell surface area is calculated to be ~46·8 $m^2\ g^{-1}$. The pore size distribution calculated from the adsorption branch using the BJH method shows that the porous Co_3O_4 microplates have an average pore size of ~18·9 nm.

Figure 6*a* presents the discharge–charge curves of the obtained porous Co_3O_4 microplates in a voltage window of 3·0–0·01 V at different current rates. During the discharge at a current rate of 0·1 C, the voltage rapidly drops to ~1·0 V with a long plateau and then declines to the cutoff voltage of 0·01 V, which is characterised by the reversible redox reaction mechanism expressed by the reaction equation[31]

$$Co_3O_4 + 8Li^+ + 8e \underset{\text{charge}}{\overset{\text{discharge}}{\rightleftharpoons}} 3Co + 4Li_2O$$

The long plateaus can be ascribed to the conversion from Co_3O_4 to the intermediate phase CoO(or $Li_xCo_3O_4$) and then to metallic Co.[32] The initial discharge capacity of ~1536 mAh g^{-1} is significantly larger than the theoretical value of bulk Co_3O_4

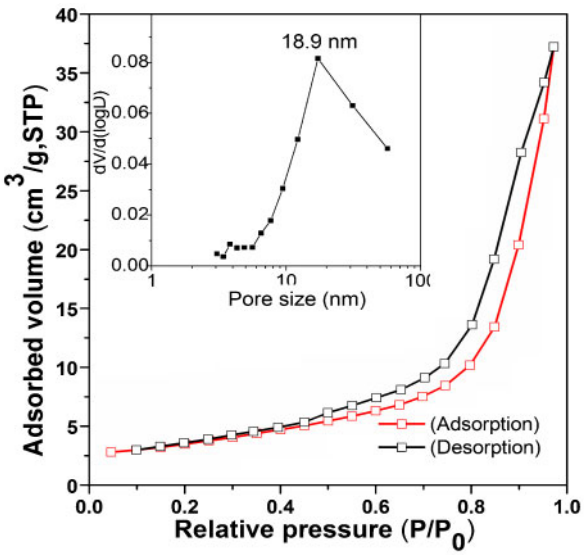

5 **N_2 adsorption/desorption isotherms and pore size distribution (inset) of porous Co_3O_4 products**

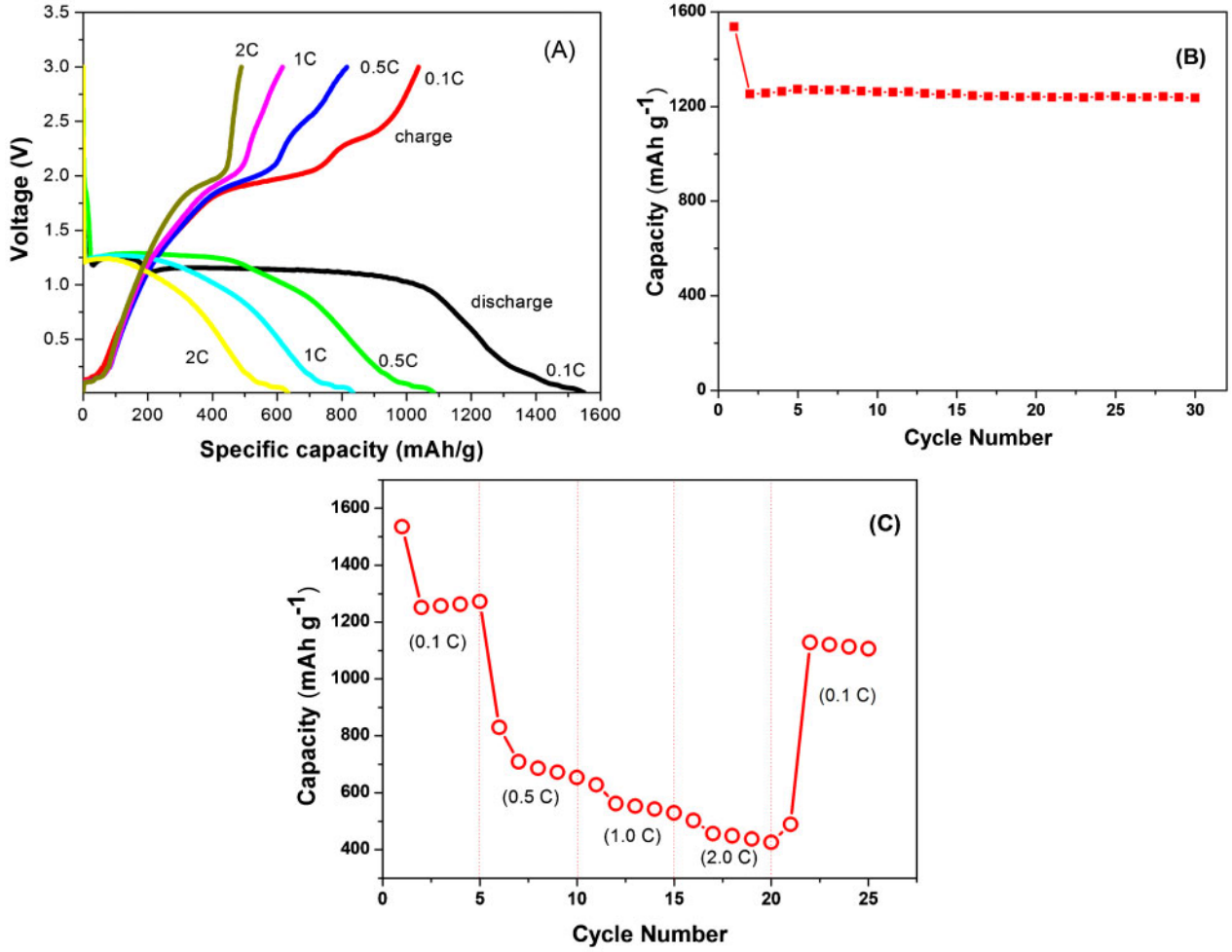

6 ***a*** **discharge–charge curves,** ***b*** **cycling performances at 0·1 C and** ***c*** **at different current densities of obtained porous Co_3O_4 microplates**

(892 mAh g^{-1}), which can be generally attributed to the formation of solid electrolyte interface layer and interfacial lithium storage.[33] This also suggests an advantage of porous Co_3O_4 microplates, in which more active sites are supplied for the intercalation of Li^+. The corresponding charge capacity is ~1050 mAh g^{-1}, meaning an irreversible capacity loss of 486 mAh g^{-1} with a Coulombic efficiency of 68·4%. This is due to the formation of solid electrolyte interface and the irreversible processes. With increase in the current rates, the corresponding discharge and charge capacity decrease in sequence.

In order to better understand the electrochemical properties of porous Co_3O_4 microplates, we also perform the cycling discharge–charge tests at 0·1 C and different current rates. As is shown in Fig. 6*b*, after the first discharge–charge cycle, the capacities of subsequent cycles are basically retained at ~1240 mAh g^{-1} up to 30 cycles. In addition, it can be calculated from the profile that the average discharge capacity is 1316 mAh g^{-1} at 0·1 C, 710 mAh g^{-1} at 0·5 C, 563 mAh g^{-1} at 1·0 C, and 454 mAh g^{-1} at 2·0 C respectively as is shown in Fig. 6*c*. Upon turning the current rate back to 0·1 C, the discharge capacity of 1183 mA g^{-1} is retrieved, indicative of high structure stability. These results indicate that the porous Co_3O_4 microplates have an excellent Li storage property. This can be well understood by the reason that the inner porous network existing among Co_3O_4 provides more pathways promoting the diffusion of electrolyte and shortening the transfer length of Li ions.

Conclusions

In summary, porous Co_3O_4 microplates have been successfully synthesised via the thermal decomposition from cobalt oxalate complex precursors with plate-like morphologies. The current method is easily conducted and suitable for inexpensive and large scale production of porous Co_3O_4 microplates. The obtained porous Co_3O_4 microplates exhibit excellent Li storage performances when used as anode materials for LIBs.

Acknowledgement

The authors gratefully acknowledge the financial supports from the National Natural Science Foundation of China (grant no. 21206025).

References

1. Z. Li, Q. Zhao, W. Fan and J. Zhan: *Nanoscale*, 2011, **3**, 1646.
2. D. Sun, P. G. Yin and L. Guo: *Acta Phys. Chim. Sinica*, 2011, **27**, 1543.
3. Y. Sun, X. Hu, W. Luo and Y. Huang: *J. Mater. Chem.*, 2012, **22**, 19190.
4. H. Xu, G. Zhu, D. Zheng, C. Xi, X. Xu and X. Shen: *J. Colloid Interface Sci.*, 2012, **383**, 75.

5. Y. Liu, C. Yu, W. Dai, X. Gao, H. Qian, Y. Hu and X. Hu: *J. Alloys Compd*, 2013, 551, 440.
6. L. Cao, M. Lu and H. Li: *J. Electron. Chem. Soc.*, 2005, **152**, A871.
7. X. Xie, Y. Li, Z. Liu, M. Haruta and W. Shen: *Nature*, 2009, **458**, 746.
8. C. Liu, C. Chen and J. Liu: *Sens. Actuators B*, 2009, **137B**, 700.
9. J. Pal and P. Chauhan: *Mater. Charact.*, 2010, **61**, 575.
10. N. Yan, L. Hu, Y. Li, Y. Wang, H. Zhong, X. Hu, X. Kong and Q. Chen: *J. Phys. Chem. C*, 2012, **116C**, 7227.
11. J. Wang, N. Yang, H. Tang, Z. Dong, Q. Jin, M. Yang, D. Kisailus, H. Zhao, Z. Tang and D. Wang: *Angew. Chem. Int. Ed.*, 2013, **52**, 1.
12. Y. Li, B. Tan and Y. Wu: *J. Am. Chem. Soc.*, 2006, **128**, 14258.
13. N. Du, H. Zhang, B. D. Chen, J. B. Wu, X. Y. Ma, Z. H. Liu, Y. Q. Zhang, D. R. Yang, X. H. Huang and J. P. Tu: *Adv. Mater.*, 2007, **19**, 4505.
14. R. Xu, J. Wang, Q. Li, G. Sun, E. Wang, S. Li, J. Gu and M. Ju: *J. Solid State Chem.*, 2009, **182**, 3177.
15. L. Tian, H. Zou, J. Fu, X. Yang, Y. Wang, H. Guo, X. Fu, C. Liang, M. Wu, P. K. Shen and Q. Gao: *Adv. Funct. Mater.*, 2010, **20**, 617.
16. J. S. Chen, T. Zhu, Q. H. Hu, J. Gao, F. Su, S. Z. Qiao and X. W. Lou: *ACS Appl. Mater. Interfaces*, 2010, **2**, 3628.
17. G. L. Zhang, D. Zhao, P. Z. Guo, Z. B. Wei and X. S. Zhao: *Acta Phys. Chim. Sinica*, 2012, **28**, 387.
18. X. Chen, J. P. Cheng, Q. L. Shou, F. Liu and X. B. Zhang: *Cryst. Eng. Commun.*, 2012, **14**, 1271.
19. N. Dahal, I. A. Ibarra and S. M. Humphery: *J. Mater. Chem.*, 2012, **22**, 12675.
20. H. W. Kim, Y. H. Jin, S. D. Seo, S. H. Lee and D. W. Kim: *ACS Nano*, 2011, **5**, 443.
21. S. K. Meher and G. R. Rao: *J. Phys. Chem. C*, 2011, **115C**, 15646.
22. A. Rumplecker, F. Kleitz, E. L. Salabas and F. Schüth: *Chem. Mater.*, 2007, **19**, 485.
23. W. Li, L. Xu and J. Chen: *Adv. Funct. Mater.*, 2005, **15**, 851.
24. F. Teng, W. Yao, Y. Zheng, Y. Ma, T. Xu, G. Gao, S. Liang, Y. Teng and Y. Zhu: *Talanta*, 2008, **76**, 1058.
25. C. C. Li, X. M. Yin, Q. H. Li, L. B. Chen and T. H. Wang: *Chem. Eur. J.*, 2011, **17**, 1596.
26. G. Binotto, D. Larcher, A. S. Prakash, R. H. Urbina, M. S. Hegde and J. M. Tarascon: *Chem. Mater.*, 2007, **19**, 3032.
27. B. Wang, T. Zhu, H. B. Wu, R. Xu, J. S. Chen and X. W. Lou: *Nanoscale*, 2012, **4**, 2145.
28. C. Sun, S. Rajasekhara, Y. Chen and J. B. Goodenough: *Chem. Comm.*, 2011, **47**, 12852.
29. X. Wang, X. Y. Chen, L. S. Gao, H. G. Zheng, Z. D. Zhang and Y. T. Qian: *J. Phys. Chem. B*, 2004, **108B**, 16401.
30. D. Wang, Q. Wang and T. Wang: *Inorg. Chem.*, 2011, **50**, 6482.
31. P. Poizot, S. Laruelle, S. Grugeon, L. Dupont and J. M. Tarascon: *Nature*, 2000, **407**, 496.
32. D. Larcher, G. Sudant, J. B. Leriche, Y. Chabre and J. M. Tarascon: *J. Electrochem. Soc.*, 2002, **149**, A234.
33. G. Binotto, D. Larcher, A. S. Prakash, R. H. Urbina, M. S. Hegde and J. M. Tarascon: *Chem. Mater.*, 2007, **19**, 3032.